J Mol Model (2013) 19:2399–2412
DOI 10.1007/s00894-013-1780-5

ORIGINAL PAPER

Prodrugs for masking bitter taste of antibacterial drugs—a computational approach

Rafik Karaman

Received: 22 November 2012 / Accepted: 21 January 2013 / Published online: 19 February 2013

Abstract DFT calculations for the acid-catalyzed hydrolysis of several maleamic acid amide derivatives revealed that the reaction rate-limiting step is determined on the nature of the amine leaving group. Further, it was established that when the amine leaving group was a secondary amine, acyclovir or cefuroxime moiety the tetrahedral intermediate formation was the rate-limiting step such as in the cases of acyclovir **ProD 1- ProD 4** and cefuroxime **ProD 1- ProD 4**. In addition, the linear correlation between the calculated and experimental rates provided a credible basis for designing prodrugs for masking bitter taste of the corresponding parental drugs which have the potential to release the parent drug in a sustained release fashion. For example, based on the DFT calculated rates the predicted $t_{1/2}$ (a time needed for 50 % of the reactant to be hydrolyzed to products) for cefuroxime prodrugs, cefuroxime **ProD 1- ProD 4**, were 12 min, 18 min, 200 min and 123 min, respectively.

Keywords Antibacterial prodrugs · Cefuroxime prodrugs · DFT calculations · Intramolecular amide hydrolysis · Maleamic acid amides · Masking bitter taste

Introduction

Taste, smell, texture and after taste are important factors in the development of dosage forms. These are important factor in product preference. Good flavor and texture are found to significantly affect sells of the product. The major factor of concern while dealing with pediatric therapies is patient's compliance. Pediatric patients tend to become uncooperative during the administration of oral medication; the most common reason being the taste of the oral formulation administered among the children. Most of the antibiotics, multivitamins and other medicines administered orally have a bitter taste making them unpleasant for children to consume.

Organoleptic properties, such as taste, are the major factors when selecting a certain drug from the generic products available in the market having the same active ingredient. Nowadays, the pharmaceutical industry is recognizing the importance of taste masking and a significant number of techniques have been developed for concealing the objectionable taste [1].

Compounds dissolve in saliva and bind to taste receptors on the tongue to provide a sweet, salty, bitter, sour, or savory sensation. Sour and sweet taste receptors are located on the tip and lateral borders of the tongue respectively. Bitter taste is sensed by the receptors concentrated on the posterior part of the tongue and savory taste receptors are distributed in areas all over the tongue. The sensation is the result of signal transduction from taste receptors located in areas known as taste buds [2]. Bitter taste molecules [3–7] are very diverse in their chemical structure and physicochemical properties [8, 9]. In humans, bitter taste perception is mediated by 25 G-protein coupled receptors of the hTAS2R gene family [10–16].

The techniques most commonly used for accomplishing taste masking include various chemical and physical methods that prevent the drug substance from interaction with the taste receptors. The simplest technique involves use of flavor enhancers. Where these methods fail more complex methodologies are adopted. Several approaches have been investigated and have resulted in the development of

Electronic supplementary material The online version of this article (doi:10.1007/s00894-013-1780-5) contains supplementary material, which is available to authorized users.

R. Karaman (✉)
Bioorganic Chemistry Department, Faculty of Pharmacy, Al-Quds University, Box 20002, Jerusalem, Palestine
e-mail: dr_karaman@yahoo.com

efficient techniques for masking a compound's bitter taste [17]. All of the developed techniques are based on a physical modification of the formulation containing the bitter tastant. Some of these techniques include: (1) coating is one of the most efficient and commonly used taste masking techniques[18]; (2) microencapsulation processes used are commonly based on the principle of solvent extraction or evaporation [19]; (3) taste masking with flavors, sweeteners, and amino acids [20]; (4) taste masking with lipophilic vehicles such as lipids, lecithin, and lecithin- like substances [21]; (5) sweeteners are generally used in combination with other taste masking technologies. [22]; (6) taste suppressants and potentiators, such as Linguagen's bitter blockers (e.g., adenosine monophosphate), are used for masking the bitter taste of various compounds by competing with binding to the G-protein coupled receptor sites (GPCR) [23]; (7) pH modifiers [24]; (8) adsorbates [25]; (9) resins [26, 27] and (10) inclusion complexes [28].

Although the mentioned approaches have helped to improve the taste of some drugs formulations, the problem of the bitter taste of drugs in pediatric and geriatric formulations still creates a serious challenge to pharmacists. Thus, different strategies should be developed in order to overcome this serious problem.

The novel chemical approach to be discussed in this paper involves the design of prodrugs for masking bitter taste of pharmaceuticals based on intramolecular processes using density functional theory (DFT) methods [29] and correlations of experimental and calculated reactions rates. No enzyme is needed to catalyze the interconversion of a prodrug to its corresponding drug. The rate of drug release is controlled by the nature of the linker bound to the drug. Bitter tastant molecules interact with taste receptors on the tongue to give bitter sensation. Altering the ability of the drug to interact with bitter taste receptors could reduce or eliminate its bitterness. This could be achieved by an appropriate modification of the structure and the size of a bitter compound. Bitter molecules bind to the G-protein coupled receptor-type T2R on the apical membrane of the taste receptor cells located in the taste buds. In humans, about 25 different T2R's are described. Additionally, several alleles are known and about 1000 different bitter phenotypes exist in human beings [30, 31].

Due to the large variation of structural features of bitter tasting molecules, it is difficult to generalize the molecular requirements for bitterness. Nevertheless, it was reported that a bitter tastant molecule requires a polar group and a hydrophobic moiety. A quantitative structure activity relationship (QSAR) model was developed and has been established for the prediction of bitterness of several tastant analogues. For example, it was reported that the addition of a pyridinium moiety to an amino acid chain of a variety of bitter amino acid compounds decreases bitterness, such as in the case of glycine. Other structural modifications, such as an increase in the number of amino groups/residues to more than three and a reduction in the poly-hydroxyl group/COOH, have been proven to decrease bitterness significantly. Moreover, changing the configuration of a bitter tastant molecule by making isomer analogues was found to be important for binding affinity to enhance bitterness agonist activity (e.g., L-tryptophan is bitter while D-tryptophan is sweet) [32].

Unraveling the mechanism of proton transfer between two oxygens in Menger's rigid carboxylic amides [33] has led to the design of prodrugs that mask the bitter taste of atenolol and dopamine. The role of the linker in these prodrugs was to block the free amine group in the corresponding parental drug which is believed to be responsible for the bitterness of the drugs as well as to enable the release of a drug in a programmable manner [34–39]. For example, the DFT calculations demonstrated that the efficiency in proton transfer between two oxygens in Kirby's N-alkylmaleamic acids and in a proton transfer between two oxygens in Menger's rigid carboxylic amides is largely sensitive to the strain energy difference between the intermediate and the reactant, the distance between the nucleophile and electrophile, and the attack angle by which the approach step commences. Using the correlation equations from the plots of the calculated and experimental effective molarity (EM) values for the above mentioned processes, the $t_{1/2}$ (time needed to convert 50 % of a prodrug to its parental drug) for several prodrugs that mask bitter tastants was calculated [34–41].

Most of the antibacterial agents used in the market suffer unpleasant taste and many of them are characterized with bitter taste. For example, cefuroxime axetil has an extremely bitter and unpleasant taste which is difficult to mask. This is a particular problem in geriatric patients who cannot swallow whole tablets or when small doses are required. Even the cefuroxime axetil suspension is difficult for pediatrics to administer due to its better and unpleasant taste [42–48].

It is believed that the extremely bitter and unpleasant taste of cefuroxime axetil is due to formation of intermolecular force/s between this drug and the active site of the bitter taste receptors. The intermolecular bond/s is/are most likely due to formation of either the hydrogen bond or ionic bond of the amido group at position 3 and the active site of the bitter taste receptors.

Cefuroxime axetil is an orally active drug though its absorption is incomplete. Its bioavailability ranges between 25 to 52 %. The axetil moiety is metabolized to acetaldehyde and acetic acid. Peak plasma concentration is reported about 2 to 3 h after an oral dose. Up to 50 % of cefuroxime in the circulation is bound to plasma proteins. The plasma half life is about 70 min and is prolonged in patients with renal impairments and in neonates. Cefuroxime axetil is

widely distributed in the body including plural fluid, sputum bone synovial fluid, and aqueous humour, but only achieves therapeutic concentration in the CSF when the meninges are inflamed. It crosses the placenta and has been detected in breast milk. Cefuroxime is excreted unchanged, by glomerular filtration and renal tubular secretion, and high concentration is achieved in urine [49].

Based on our previously reported DFT calculations and on experimental data for the acid-catalyzed hydrolysis of amide acids **1**–**12** (Scheme 1) [50, 51], four cefuroxime prodrugs are proposed (Scheme 2). As shown in Scheme 2, the cefuroxime prodrugs, **ProD 1** - **ProD 4** molecules are composed of an amide acid linker, containing a carboxylic acid group (hydrophilic moiety) and the rest of the antibacterial prodrug molecule (a lipophilic moiety). The combination of hydrophilic and lipophilic groups provides a prodrug moiety with a potential to be with a high permeability (a moderate HLB). It is worth noting, that a hydrophilic lipophylic balance value of the prodrug molecule will be dependent on the pH of the target physiologic environment. In the stomach (pH 1–2), it is expected that prodrugs, cefuroxime **ProD 1** – **ProD 4** will be in a free carboxylic acid form (a relatively high lipophilicity) whereas in the blood stream circulation (pH 7.4) a carboxylate anion form (a relatively low lipophilicity) is expected to be predominant. Our strategy is to prepare cefuroxime **ProD 1- ProD 4** (Scheme 2) as sodium or potassium carboxylates due to their high stability in neutral aqueous medium. It should be indicated that compounds **1**–**12** undergo a relatively fast hydrolysis in acidic aqueous medium whereas they are quite stable at pH 7.4.

In this paper, we report a DFT computational study on intramolecular acid-catalyzed hydrolysis for four different cefuroxime prodrugs, **ProD 1- ProD 4** (Scheme 2). Based on the calculated and experimental rates for the hydrolysis of **1**–**12**, the $t_{1/2}$ values for **ProD 1- ProD 4** were evaluated.

The aim of this work was to design various cefuroxime prodrugs with the potential to be tissue permeable, lack the bitterness of their parental drug and have the capability to chemically and not enzymatically undergo hydrolysis in physiological environment to furnish cefuroxime in a sustain release manner.

Calculations methods

The Becke three-parameter, hybrid functional combined with the Lee, Yang, and Parr correlation functional, denoted B3LYP, were employed in the calculations using density functional theory (DFT). All calculations were carried out using the quantum chemical package Gaussian-2009 [52]. Calculations were carried out based on the restricted Hartree-Fock method [52]. The starting geometries of all calculated molecules were obtained using the Argus Lab program [53] and were initially optimized at the HF/6-31G level of theory, followed by optimization at the B3LYP/6-31G(d,p). Total geometry optimizations included all internal rotations. Second derivatives were estimated for all 3N-6 geometrical parameters during optimization. The search for the global minimum structure in each of the systems studied was accomplished by 360° rotation of the carboxylic group about the bond C6-C7 (i.e., variation of the dihedral angle O1/C7/C6/C5, Chart 1), and 360° rotation of the carbonyl amide group about the C4-C5 bond (i.e., variation of the dihedral angle O3/C4/C5/C6) in increments of 10° and calculation of the conformational energies (see Chart 1). For conservation of computer time, the DFT calculations for cefuroxime **ProD 1- ProD 4** were run on molecules by which the furyl-2-methoxyimino group was replaced with a methyl group. It is expected that such modification will not affect the activation energy values for the entities involved in the process. For systems **1**–**12**, acyclovir **ProD 1- ProD 4** and cefuroxime **Prod 1-ProD 4** two types of conformations in particular were considered: one in which the amide carbonyl is *perpendicular* to the carboxyl carbonyl group and another in which it is *planar*. An energy minimum (a stable compound or a reactive intermediate) has no negative vibrational force constant. A transition state is a saddle point which has only one negative vibrational force constant [54]. Transition states were located first by the normal reaction coordinate method [55] where the enthalpy changes was monitored by stepwise changing the interatomic distance between two specific atoms. The geometry at the highest point on the energy profile was re-optimized by using the energy gradient method at the B3LYP/6-31G(d,p) level of theory [52]. The "reaction coordinate method" [55] was used to calculate the activation energy in all maleamic (4-amino-4-oxo-2butenoic) acids (Schemes 1 and 2). In this method, one bond length is constrained for the appropriate degree of freedom while all other variables are freely optimized. The activation energy values for the approach processes (the approach of O1 toward C4, Chart 1) were calculated from the difference in energies of the global minimum structures (GM) and the derived transition states (tetrahedral intermediate formation, Scheme 3). Similarly, the activation energies of the dissociation processes (the breakdown of C4-N9 bond, Chart 1) were calculated from the difference in energies of the global minimum structures (GM) and the corresponding transition states (tetrahedral intermediate breakdown, Scheme 3). Verification of the desired reactants and products was accomplished using the "intrinsic coordinate method" [55]. The transition state structures were verified by their only negative frequency. Full optimization of the transition states was accomplished after removing any constrains imposed while executing the energy profile. The activation energies obtained from the DFT at B3LYP/6-31G(d,p) level of theory for all molecules were calculated with and without the inclusion of solvent (water and ether). The calculations with the incorporation of a solvent were performed using the integral

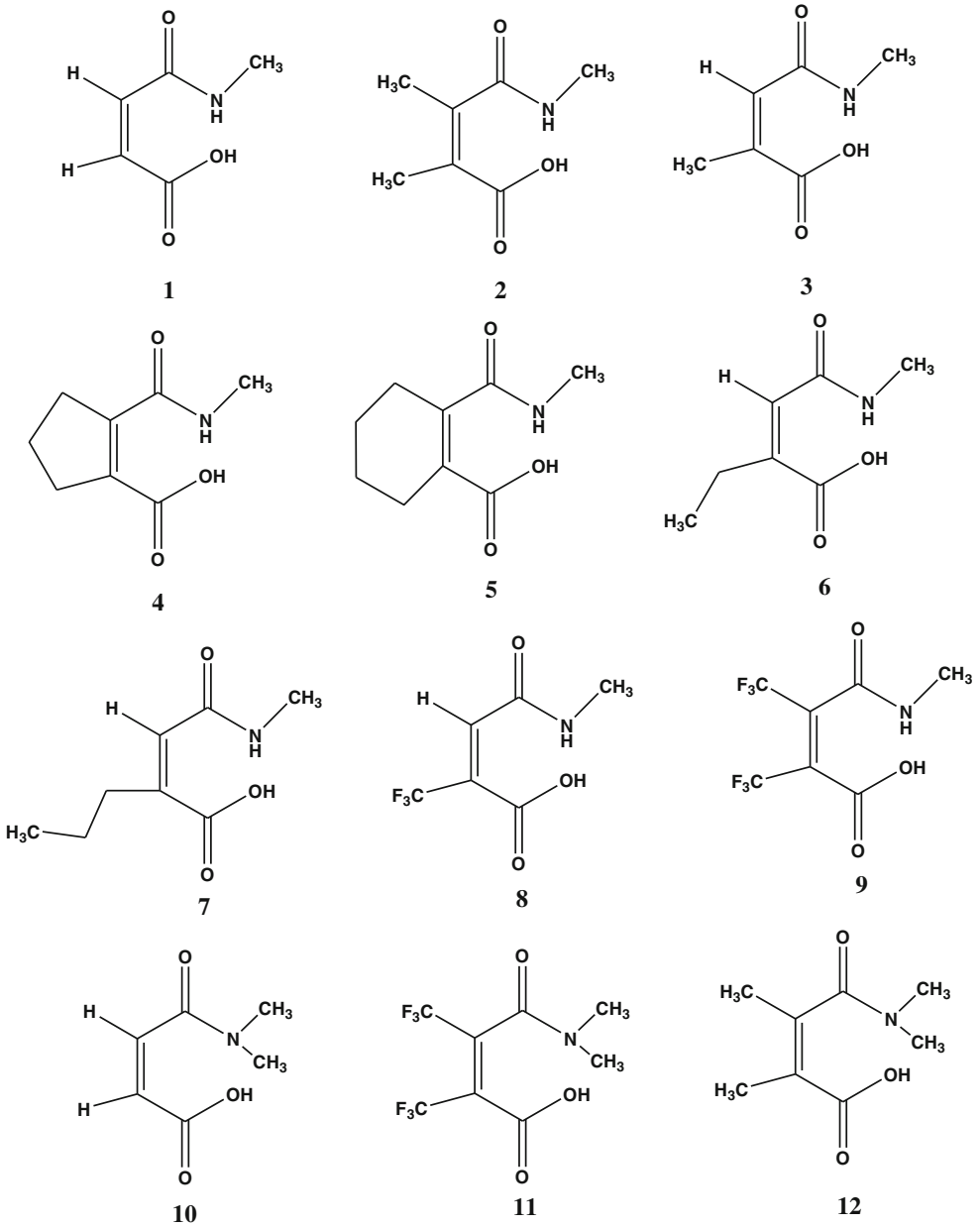

Scheme 1 Chemical structures for **1**–**12**

equation formalism model of the polarizable continuum model (PCM) [56–59]. In this model the cavity is created via a series of overlapping spheres. The radii type employed was the united atom topological model on radii optimized for the PBE0/6-31G(d) level of theory.

Results and discussion

Kirby and coworkers have investigated the structural factors associated with the high reactivity in the intramolecular acid-catalyzed hydrolysis of seven maleamic (4-amino-4-oxo-2butenoic) acids, **1**–**7** (Scheme 1) [50, 60]. Their findings indicate that the efficiency of the intramolecular hydrolysis is remarkably sensitive to the pattern of substitution on the carbon-carbon double bond and the rate of the hydrolysis of the amide acid derivatives studied ranges over more than ten powers of ten. In addition, their study revealed that the amide bond cleavage is due to intramolecular nucleophilic catalysis by the adjacent carboxylic acid group and the dissociation of the tetrahedral intermediate is the rate-limiting step [50]. Later on Kluger studied the intramolecular hydrolysis mechanism of eight maleamic acids derived from aliphatic amines of a wide range of basicity [61]. His

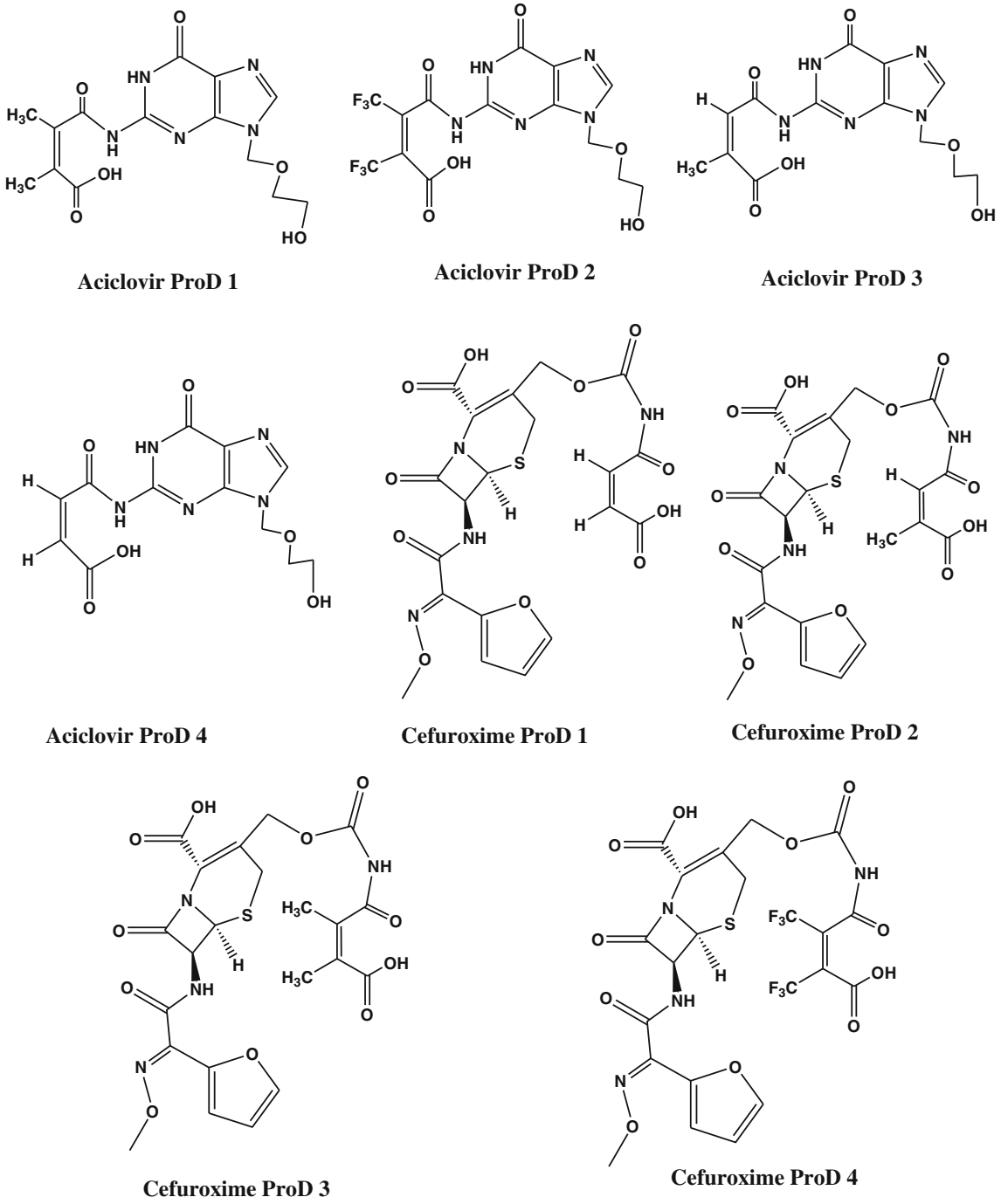

Scheme 2 Chemical structures for acyclovir **ProD 1- ProD 4** and cefuroxime **ProD 1- ProD 4**

study concluded that the identity of the rate-limiting step is a function of both the basicity of the leaving group and the acidity of the solution.

In order to exploit systems **1**–**12** as prodrug linkers for cefuroxime and other important drugs we have recently unraveled the mechanism for their acid-catalyzed hydrolysis using DFT calculation methods. In accordance with the reports by Kirby [50] and Kluger [61] we have found that the hydrolysis proceeds by one mechanism, however, the rate-limiting step for the process was found to be largely dependent on the nature of the amine leaving group. Two different steps were proposed as rate-limiting: (1) a step involving the formation of a tetrahedral intermediate [62], and (2) a step involving tetrahedral intermediate dissociation to furnish products (Scheme 3) [55].

Similar to that done for systems **1**–**12**, the DFT calculations for the acid-catalyzed hydrolysis of cefuroxime prodrugs **ProD 1- ProD 4** were directed toward elucidation of the transition and ground state structures (reactants, intermediates and

products). Calculations for all entities were conducted in water and the gas phase. It is expected that the stability of the ground and transition states will be different in solvent having low dielectric constant, such as the gas phase and solvent with high dielectric constant, such as water.

General consideration

The carboxylic acid amide moiety could be engaged in inter- or intramolecular hydrogen bonding. Therefore the free energy of the reactant is strongly dependent on its conformation. We were concerned with the identification of the most stable conformation (global minimum, GM) for each of cefuroxime **ProD 1-ProD 4**. The search for the global minimum structures for all acid amides (cefuroxime **ProD 1-ProD 4**) was accomplished by 36 rotations of the carboxyl group about the bond C6-C7 in increments of 10° (i.e., variation of the dihedral angle O1/C7/C6/C5, see Chart 1), and 360° rotation of the carbonyl amide group about the bond C4-C5 (i.e., variation of the dihedral angle O3/C4/C5/C6) in increments of 10° and calculation of the conformational energies (see Chart 1).

In the DFT calculations of the starting geometries in cefuroxime **ProD 1- ProD 4**, two different types of conformations were considered: one in which the amide carbonyl is *perpendicular* to the carboxyl group and another in which it is *planar* (Chart 1). It was found that the global minimum structures for cefuroxime **ProD 1- ProD 4** all exist in a *perpendicular* conformation (see Fig. 1). This is similar to that found for the global minimum structures of **1**–**12**.

Optimized structures for the molecules involved in the acid-catalyzed hydrolysis of cefuroxime ProD 1- ProD 4

Global minimum structures (GM)

The global minimum structures for **ProD 1GM-ProD 4GM** are shown in Fig. 1. Examination of the calculated geometries in Fig. 1 indicates that all the reactants exhibit conformations by which the carboxyl group is engaged intramolecularly in a hydrogen bond to form a cyclic ring. However, the size of the ring is dependent on the nature of the substituents on the C-C double bond of the maleic acid moiety. In addition, the calculated values for angles α and β in the global minimum structures were in the range of 121.4–130.8° and 117.8–123.6°, respectively.

*Transition state geometries for the tetrahedral intermediate formation (***TSf***)*

The calculated DFT optimized structures for the transition states of the tetrahedral intermediate formation in **ProD 1- ProD 4** (**ProD 1TS$_2$- ProD 4TS$_2$**) are illustrated in Fig. 2. Inspection of the transition state DFT optimized structures (**TS$_f$**) indicates that all of them resemble that of the corresponding reactants (global minimum structures). Furthermore, the calculated C-O distance (the distance between the nucleophile O- and the electrophile C, in all the transition states was 2.30 Å. The angles α and β were quite similar to that of the corresponding global minimum structures, and were in the range 118.0–120.5° and 118.1–118.8°, respectively. In addition, the transition state structures were found to exhibit conformation by which the carboxylic group and the neighboring β-lactam carbonyl oxygen are engaged in intramolecular hydrogen bond to form six-membered ring. The calculated hydrogen bond was in the range 1.63−1.64 Å.

*Tetrahedral intermediate geometries (***INT2***)*

The optimized structures for the tetrahedral intermediate, **ProD 1INT$_2$- 4INT$_2$**, are shown in Fig. 3. Careful examination of the structures reveals that angles α and β values in the intermediates are reduced when compared to that of the corresponding reactants. The α values were found in the range 108.3–109.6° whereas that for the β were in the range 107.4–109.4°. Furthermore, the angles around the tetrahedral carbon were found to be similar to that of regular tetrahedral intermediates. Similarly to the transition state

Chart 1 Chemical representation of the *perpendicular* and *planar* conformations for the global minimum structures (GM)

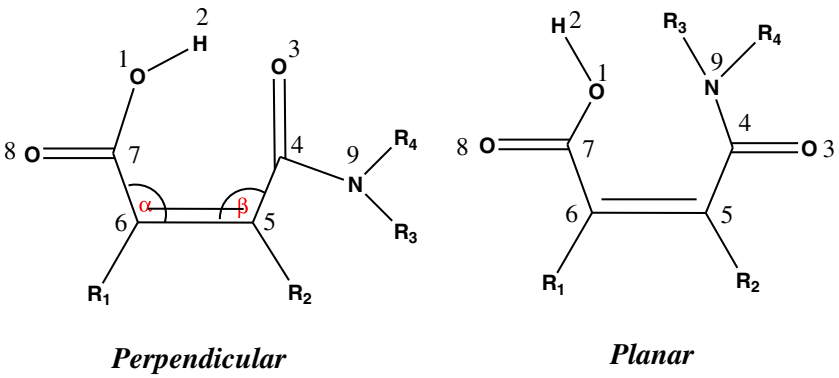

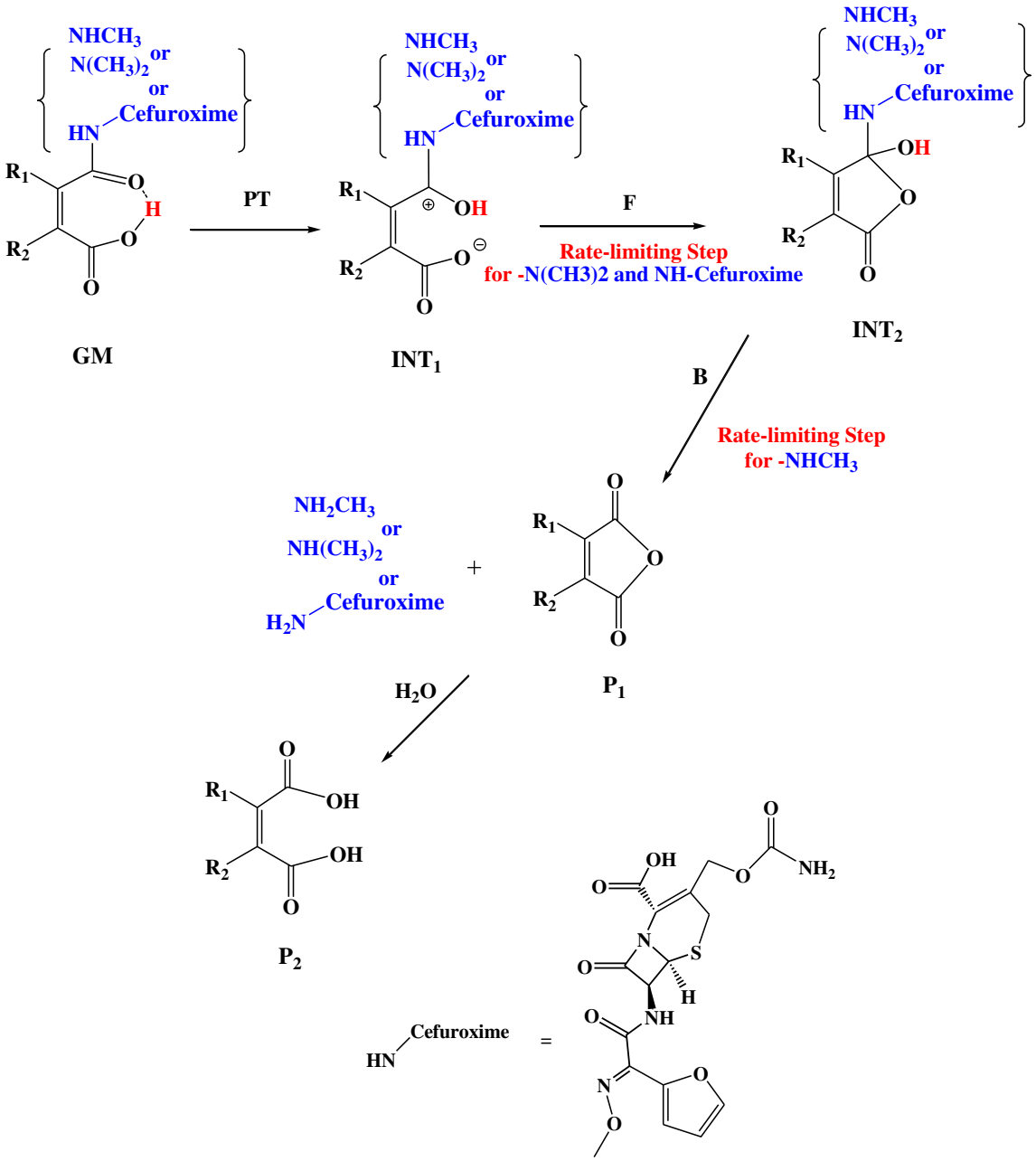

Scheme 3 Proposed mechanism for acid-catalyzed hydrolysis of N-alkylmaleamic acids. GM, INT1, INT2 P1 and P2 are global minimum structure, intermediate 1, intermediate 2 product 1 and products 2, respectively

structures, the intermediate structures were found to exhibit conformation by which the carboxylic group and the neighboring β-lactam carbonyl oxygen are engaged in intramolecular hydrogen bond to form six-membered ring. The calculated hydrogen bond was in the range 1.61–1.64 Å.

Mechanistic investigation

The DFT at B3LYP/6-31G(d,p) level of theory kinetic and thermodynamic properties for cefuroxime **ProD 1- ProD 4** (Scheme 2) were calculated using the quantum chemical package Gaussian-2009 [52]. The enthalpy and entropy energy values for all entities involved in the hydrolysis global minimum structures (GM), products (P), transition states (TS) and intermediates, (INT) were calculated in the gas phase and water. Table S1 lists the energy values for **ProD 1GM - ProD 4GM**, **ProD 1TS$_f$ - ProD 4TS$_f$** and **ProD 1INT$_f$ - ProD 4INT$_f$**, and Figs. 1, 2 and 3 show their DFT optimized structures, respectively.

Using the calculated DFT values for the enthalpy and entropy of the GM and the transition states in the hydrolysis of cefuroxime **ProD 1- ProD 4** the barriers ($\Delta G^{\ddagger}$) for all

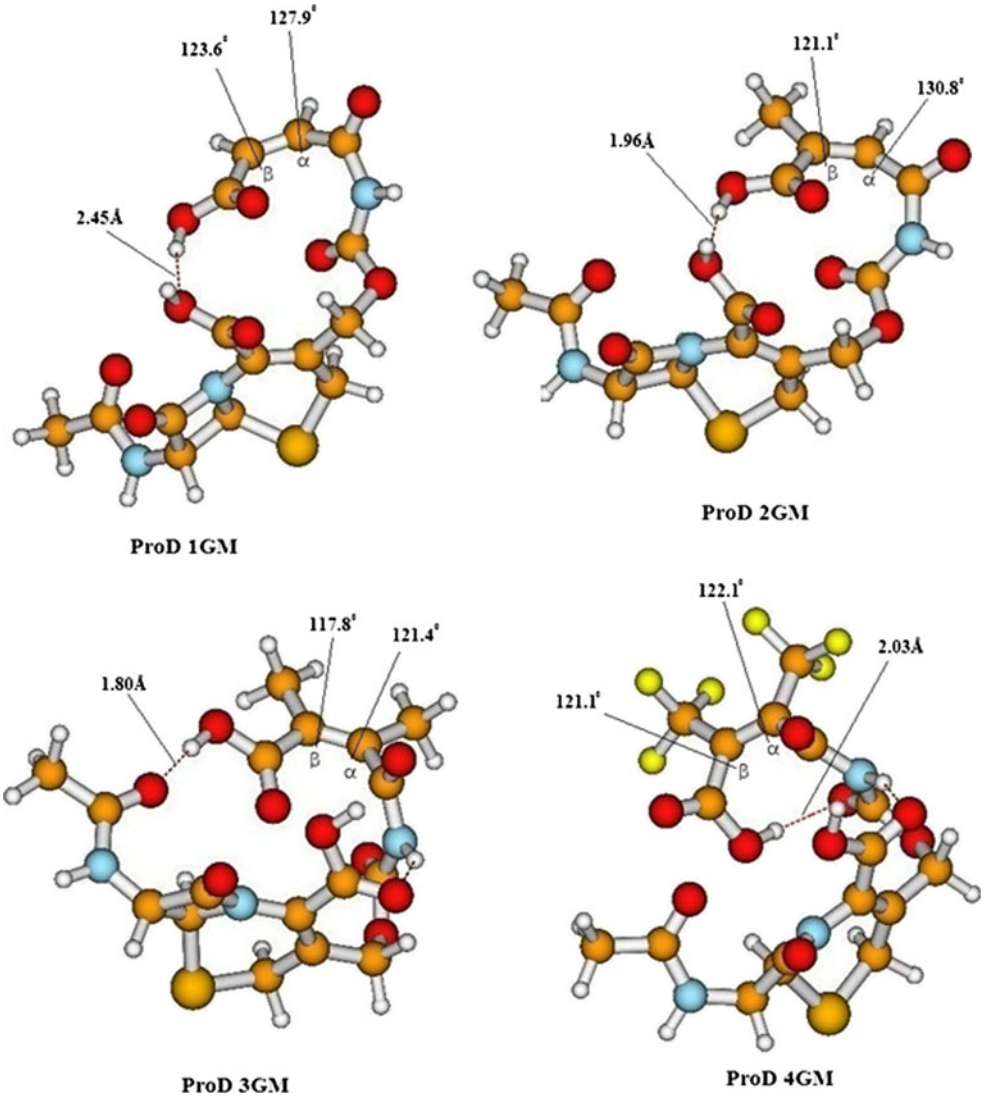

Fig. 1 DFT optimized structures for the global minimum (GM) in cefuroxime **ProD 1- ProD 4**

steps described in Scheme 3 were calculated in the gas phase as well as in a dielectric constant of 78.39 (water). The activation energy values for those barriers are summarized in Table 1. Inspection of the $\Delta G^{\ddagger}$ ($\Delta G_f^{\ddagger}$, activation energy for the tetrahedral intermediate formation and $\Delta G_b^{\ddagger}$, activation energy of the tetrahedral intermediate breakdown) values listed in Table 1 demonstrated that the rate-limiting step in the acid-catalyzed hydrolysis of cefuroxime **ProD 1- ProD 4** is the intermediate formation (Scheme 3).

In order to evaluate the factors affecting the reaction rate in cefuroxime prodrugs **ProD 1- ProD 4** we have compared their calculated properties to that previously calculated for the reactions of **1**–**12** and acyclovir **ProD 1- ProD 4**.

Table 1 lists the energy barrier for the intermediate formation ($\Delta G_f^{\ddagger}$) and breakdown ($\Delta G_b^{\ddagger}$) for systems **1**–**12** and acyclovir **ProD 1- ProD 4**. Examination of Table 1 reveals that the rate-limiting step (higher barrier) in the gas phase for all systems studied (**1**–**12** and acyclovir **ProD 1**–**4**) is the tetrahedral intermediate formation (the activation energy for the tetrahedral intermediate formation is about 5–30 kcal mol^{-1} higher than that for its breakdown). On the other hand, the picture is somewhat different when the calculations were done in dielectric constant of 78.39 (water medium). While for systems **1**–**9**, the rate-limiting step was the breakdown of the tetrahedral intermediate (energy difference between the breakdown and formation barriers is 3–8 kcal mol^{-1}) for systems **10**–**12** and acyclovir **ProD 1- ProD 4** the rate-limiting step was found to be the formation of the tetrahedral intermediate (energy difference between the formation and break-down barriers is 5–30 kcal mol^{-1}).

Based on the reaction mechanism proposed by Kirby's group and our previous calculations [50, 51], it is expected that polar and apolar solvents will have different effects on the stabilization of the entities involved in the process. The activation energies for the

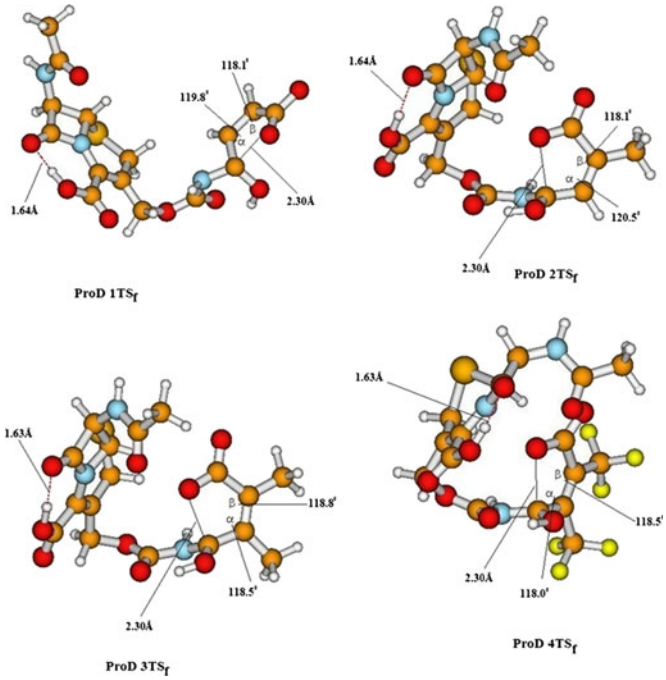

Fig. 2 DFT optimized structures for the transition state structures (TSf) in the reactions of cefuroxime **ProD 1- ProD 4**

tetrahedral intermediate formation process ($\Delta G_f^{\ddagger}$) and the tetrahedral intermediate breakdown process ($\Delta G_b^{\ddagger}$) calculated in water and the gas phase (Table 1) demonstrate that solvents with low dielectric constants such as the gas phase tend to shift the equilibrium to the reactants by destabilizing TS_f and thus making the approach as the rate-limiting step whereas solvents with high dielectric constants such as water interact via dipole-dipole interactions with the ionic transition state to shift the equilibrium to the right side. These interactions stabilize the transition state (TS_f) for the tetrahedral intermediate formation and consequently lower the approach barrier and thus the reaction rate will be dependent on the tetrahedral intermediate breakdown step.

In order to explore the factor determining the rate-limiting step, using Allinger's MM2 method [63] we have calculated the strain energy values for the reactants (GM), and intermediates (INT2) in **1**–**12**, aciclovir **ProD 1- ProD 4** and cefuroxime **ProD 1-ProD 4**. The MM2 strain energies (Es) for these structures are tabulated in Table 1. The calculated Es values were examined for correlation with the experimental relative rate (log k_{rel}) and DFT calculated activation energy values, ($\Delta G_f^{\ddagger}$ and $\Delta G_b^{\ddagger}$) (Table 1). The correlation results demonstrate a good correlation between the tetrahedral intermediates strain energy values (Es INT2) in systems **1**–**7** and the experimental relative rates (log k_{rel}) [50, 51] on one hand and the activation energies for the tetrahedral intermediate breakdown ($\Delta G_b^{\ddagger}$) on the other hand. The correlation coefficient values (R) depicted in Fig. 4a and b were 0.84 and 0.94, respectively. However, in systems **10**–**12**, acyclovir **ProD1** –**ProD 4** and cefuroxime **ProD1** – **ProD4** where the rate-limiting step was the tetrahedral intermediate formation, the DFT activation energies were found to be strongly correlated with the difference in the strain energies of the tetrahedral intermediates and their corresponding global minimum structures (Es INT-GM) with a correlation coefficient (R) of 0.90 (Fig. 4). Attempts to correlate the strain energies for the global minimum structures (Es for GM) with the experimental log k_{rel} resulted in a random correlation with R=0.20.

Figures 4a and b and Table 1 demonstrate that the reaction rate for systems **1**–**7** is dependent on the tetrahedral intermediate breakdown and its value is largely affected by the strain energy of the tetrahedral intermediate formed. Systems with less-strained intermediates such as **2** and **5** undergo hydrolysis with higher rates than that having more strained intermediates such as **4**. This might be attributed to the fact that the transition state structures in **1**–**7** resemble that of the corresponding intermediates. On the other hand, as shown in Table 1 the acid catalyzed hydrolysis rates for systems **9**–**12**, acyclovir **ProD1**-**ProD4** and cefuroxime **ProD1**-**ProD4** are solely dependent on the tetrahedral intermediate formation step (rate-limiting). The rate for systems having global minimum and intermediate structures with close similarity (Es for INT close to Es for GM) such as system **11** and Cefuroxime **ProD 4** is higher than that for processes by which the difference in the strain energies for their intermediates and the corresponding reactants (Es (INT-GM) is large such as acyclovir **ProD 1** and acyclovir **ProD 4** . This is because less energy is needed to convert a reactant to tetrahedral intermediate with similar structures.

Compounds **10**–**12,** acyclovir **ProD 1- ProD 4** and cecfuroxime **ProD 1- ProD 4** represent systems with different leaving groups by which the leaving group NHMe in **1**–**9** was replaced with more bulky groups. In the case where the leaving group is a secondary amine, $NH(CH_3)_2$, or a cefuroxime moiety the formation-break-down barriers ratio is shifted toward the formation whereas in the cases where the leaving group is a primary amine, $NHCH_3$, the amine moiety has less ability to leave due to the electron-donating effect of the methyl group. This result is in accordance with the conclusions drawn by Kluger and Chin [48].

For drawing credibility to the DFT calculations executed in this study the water calculated B3LYP/6-31G(d,p) free activation energies for the tetrahedral intermediate breakdown ($\Delta G_{BW}^{\ddagger}$) were correlated with the corresponding experimental free activation energies (Exp $\Delta G^{\ddagger}$). Strong correlation was obtained with a correlation coefficient R= 0.97 (Fig. 4).

The effective molarities (EM) for the reactions of 1–12, acyclovir ProD 1- ProD 4 and cefuroxime ProD 1 - ProD 4

The effective molarity (EM) value is commonly used as a measure for intramolecular efficiency. It is defined as a rate ratio of the intramolecular reaction and its corresponding intermolecular where both reactions are driven by the same mechanism. Values in the order of 10^9–10^{13} M have been measured for the EM in intramolecular processes occurring through nucleophilic addition. Whereas for proton transfer processes EM values of less than 10 M were reported [64, 65].

For obtaining the EM values for the reactions of **1**–**12** and cefuroxime **ProD 1**–**4** we have calculated the kinetic and thermodynamic parameters for their corresponding intermolecular process, **Inter** (Scheme 4).

Equation 5, derived from Eqs. 1–4, describes the EM term as a function of the difference in the activation energies of the intra- and the corresponding intermolecular processes. The calculated EM values for the reactions of **1**–**12**, acyclovir **ProD 1- ProD 4** and cefuroxime **ProD 1- ProD 4** as calculated by Eq. 5 are listed in Table 1.

$$EM = k_{intra}/k_{inter} \tag{1}$$

$$\Delta G^{\ddagger}_{inter} = -RT \ln\ k_{inter} \tag{2}$$

$$\Delta G^{\ddagger}_{intra} = -RT \ln\ k_{intra} \tag{3}$$

$$\Delta G^{\ddagger}_{intra} - \Delta G^{\ddagger}_{inter} = -RT \ln\ k_{intra}/k_{inter} \tag{4}$$

$$\ln\ EM = -\left(\Delta G^{\ddagger}_{intra} - \Delta G^{\ddagger}_{inter}\right)/RT \tag{5}$$

Where T is the temperature in Kelvin and R is the gas constant.

The calculated log EM values in Table 1 were correlated with the corresponding EM experimental values. The correlation equation with its correlation coefficient is shown in Eq. 6.

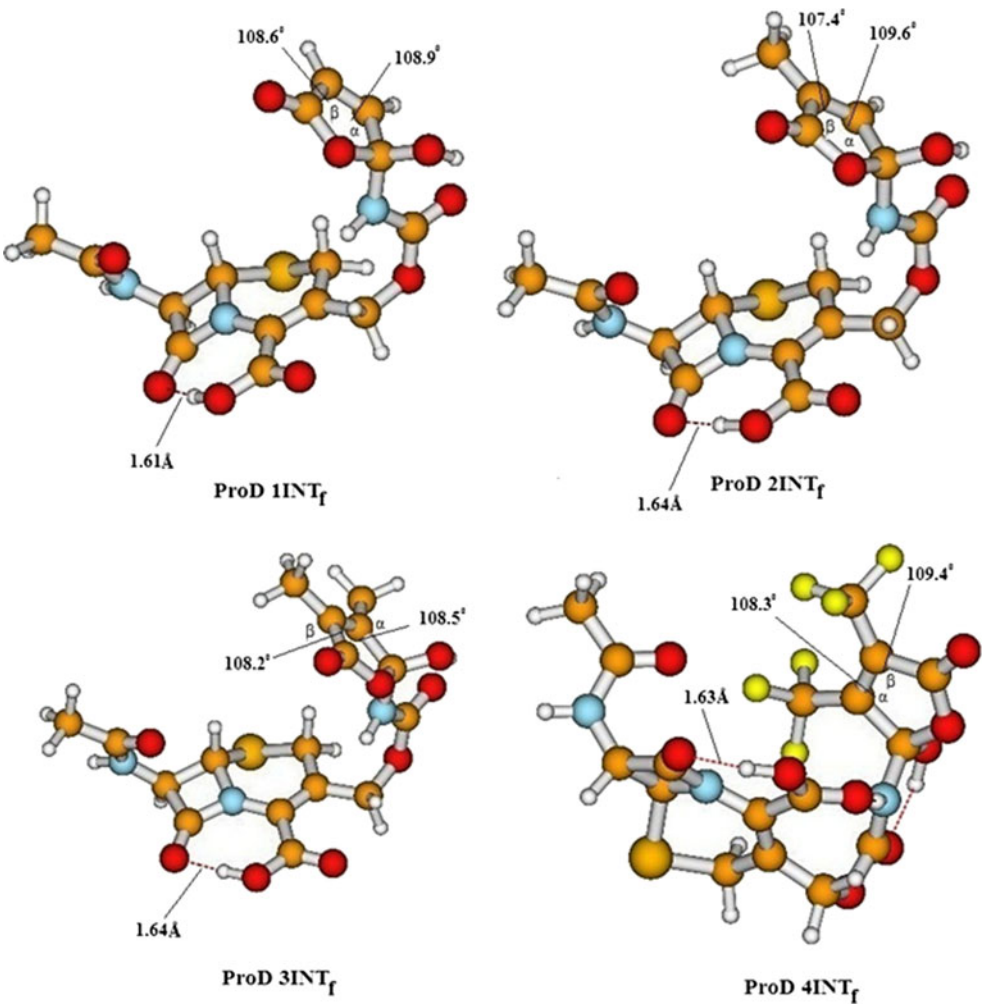

Fig. 3 DFT optimized structures for the tetrahedral intermediate INT2 (INTf) structures in the reactions of **ProD 1- ProD 4**

Table 1 DFT (B3LYP) calculated kinetic and thermodynamic properties for the acid catalyzed hydrolysis of **1**–**12**, acyclovir **ProD 1**- **ProD 4**, cefuroxime **ProD 1** – **ProD 4** and **Inter**

System	$\Delta G_{bGP}^{\ddagger}$ (kcal mol^{-1})	$\Delta G_{bW}^{\ddagger}$ (kcal mol^{-1})	$\Delta G_{fGP}^{\ddagger}$ (kcal mol^{-1})	$\Delta G_{fW}^{\ddagger}$ (kcal mol^{-1})	log k_{rel} [50]	log EM [50] (Exp)	log EM (Calc)	Es (INT_2) (kcal mol^{-1})	Es (GM) (kcal mol^{-1})
1	28.08	33.06	33.53	26.10	0	7.724	8.52	20.55	10.16
2	16.42	20.05	27.08	17.90	4.371	15.86	18.08	16.16	10.82
3	24.90	28.42	32.57	24.80	1.494	7.742	11.93	17.32	9.40
4	36.77	38.11	45.37	32.16	−4.377	1.255	4.81	27.89	12.30
5	17.41	23.12	26.87	17.89	2.732	15.190	15.82	19.25	9.18
6	23.92	27.28	32.12	23.87	1.516	6.962	12.76	17.59	5.12
7	25.03	27.55	32.3	24.40	1.648	8.568	12.57	18.55	6.20
8	24.87	30.12	32.37	23.66	–	–	6.36	22.34	12.86
9	17.24	15.15	25.94	11.97	–	–	21.68	26.92	28.29
10	4.65	24.64	26.19	29.04	–	–	11.47	26.92	28.29
11	0.66	19.02	21.07	36.41	–	–	6.06	21.56	14.15
12	2.80	8.79	24.27	22.87	–	–	16.01	19.78	25.52
Aciclovir **ProD 1**	4.93	2.07	32.83	26.46	–	–	13.36	24.71	7.13
Aciclovir **ProD 2**	8.42	0.66	34.12	31.50	–	–	9.66	29.45	32.70
Aciclovir **ProD 3**	6.02	2.26	30.53	22.96	–	–	15.94	42.27	48.80
Aciclovir **ProD 4**	3.44	2.92	34.04	25.73	–	–	13.91	31.16	35.70
Cefuroxime **ProD 1**	0	5.22	27.25	19.22	–	–	18.70	65.66	55.13
Cefuroxime **ProD 2**	4.65	3.18	22.45	19.44	–	–	18.54	60.72	56.64
Cefuroxime **ProD 3**	0.66	0.82	26.14	20.75	–	–	17.57	57.98	52.12
Cefuroxime **ProD 4**	2.80	0	21.79	20.47	–	–	17.77	64.19	60.95
Inter	–	44.65	–	–	–	–	–	–	–

B3LYP refers to values calculated by B3LYP/6-31G(d,p) method. $\Delta G^{\ddagger}$ is the calculated activation free energy (kcal mol^{-1}). Es refers to strain energy calculated by Allinger's MM2 method. GM and INT_2 refer to reactant and intermediate 2, respectively. EM = $e^{-(\Delta G^{\ddagger}inter - \Delta G^{\ddagger}intra)/RT}$. BW and FW refer to tetrahedral intermediate breakdown and tetrahedral intermediate formation calculated in water, respectively. Exp refers to experimental value. Calc refers to DFT calculated values

Careful examination of the calculated log EM values listed in Table 1 demonstrates that **2**, **5** were the most efficient processes among **1**–**9**, whereas **4** and **8** were the least. The discrepancy in rates between **2** and **5** on one hand and **4** and **8** on the other hand might be attributed to strain effects.

$$\log\ EM_{calc} = 0.81\ \log\ EM_{exp} + 4.75 \quad R^2 = 0.86 \qquad (6)$$

Calculation of the $t_{1/2}$ values for the acid catalyzed hydrolysis of cefuroxime prodrugs ProD 1-ProD 4.

Using Eqs. 7 and 8 obtained from the correlation of log k_{rel} vs. $\Delta G_b^{\ddagger}$ and $\Delta G_f^{\ddagger}$ vs. $\Delta G_b^{\ddagger}$ and the $t_{1/2}$ value for process **2**, $t_{1/2}$ about 50 min (36), we have calculated the $t_{1/2}$ values for cefuroxime **ProD 1**- **ProD 4**. The calculated $t_{1/2}$ values at pH5 for cefuroxime **ProD 1**- **ProD 4** are 12 min, 18 min, 200 min and 123 min, respectively. It should be indicated that the $t_{1/2}$ for the hydrolysis reaction of these prodrugs at higher pHs such as 6 (intestine) or 7.4 (blood circulation) will be much higher than the values at pH5.

$$\log\ k_{rel} = -0.44\ \Delta G_b^{\ddagger} + 13.53 \quad R^2 = 0.93 \qquad (7)$$

$$\Delta G_f^{\ddagger} = 1.15\ \Delta G_b^{\ddagger} + 1.11 \quad R^2 = 0.95 \qquad (8)$$

Conclusions

The DFT calculations demonstrated that the efficiency of these processes is largely sensitive to the pattern of substitution on the carbon-carbon double bond and the nature of the amide N-alkyl group. The reaction rate was found to be linearly correlated with the strain energy difference between

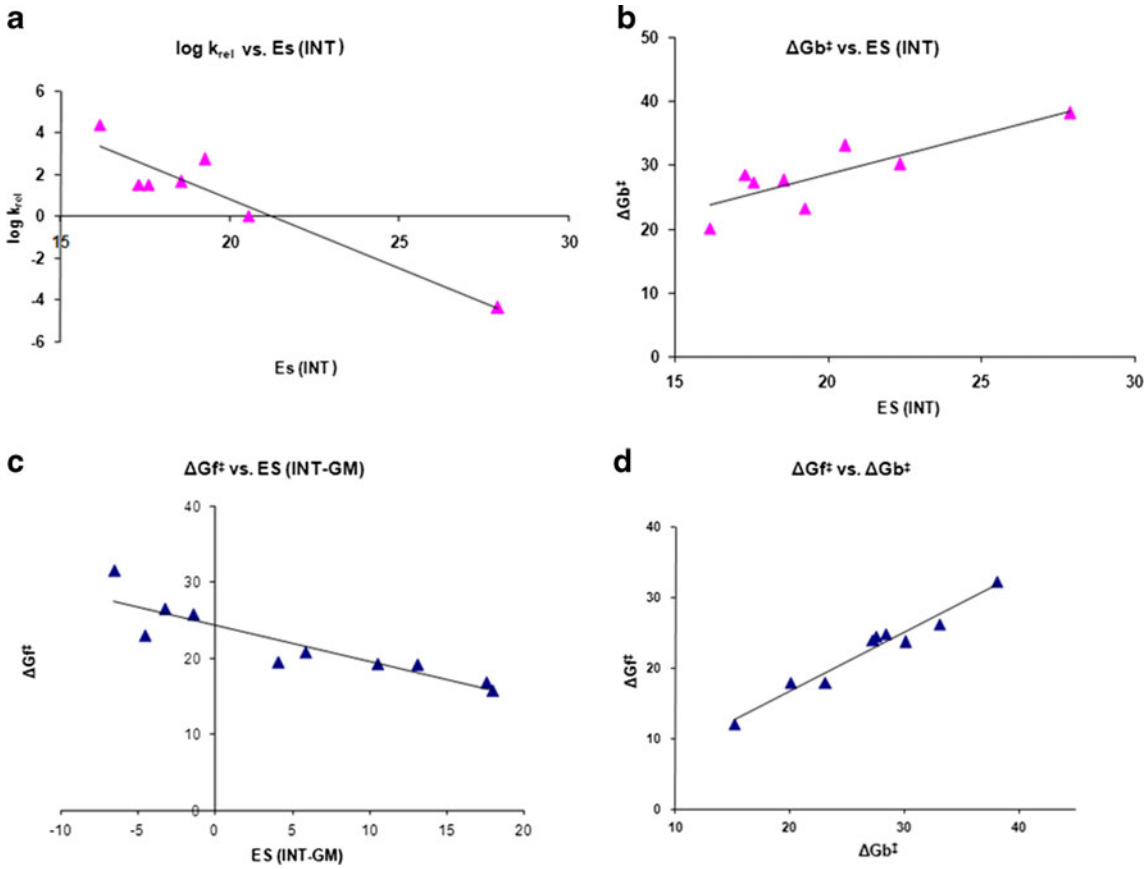

Fig. 4 **a** Plot of acid-catalyzed hydrolysis rate (log k_{rel}) vs. intermediate strain energy (Es $_{INT2}$) for processes **1**–**7**. **b** Plot of activation energy for tetrahedral intermediate breakdown $\Delta Gb^{\ddagger}$ vs. intermediate strain energy (Es $_{INT2}$) for the reactions of **1**–**8**. **c** Plot of activation energy for tetrahedral intermediate formation $\Delta Gf^{\ddagger}$ vs. strain energy difference between intermediate and reactant (Es $_{INT2\text{-}GM}$) in systems **10**–**12**, acyclovir **ProD 1**- **ProD 4** and cefuroxime **ProD 1**- **ProD 4**. **d** Plot of activation energy for tetrahedral intermediate formation $\Delta Gf^{\ddagger}$ vs. activation energy for tetrahedral intermediate breakdown $\Delta Gb^{\ddagger}$ in systems **1**–**9**

the intermediate and the reactant (E_s INT-GM). In addition, a linear correlation between the calculated and experimental EM values reinforce the credibility of using DFT methods in predicting energies as well as rates for reactions of the type described herein [66–71].

Using the correlation equation obtained from the plot of the calculated and experimental EM values we have calculated the $t_{1/2}$ of four different cefuroxime prodrugs (**ProD 1**-**ProD 4**).

It should be indicated, that although the calculated and the experimental $t_{1/2}$ values are comparable the calculation results need not be taken too literally in absolute terms since the data of interest are all comparisons.

The strategy to achieve desirable prodrugs of cefuroxime that are bitterless and capable of releasing cefuroxime in a controlled manner is: (i) synthesis of the linker and coupling of the parent drug to the linker using Kirby's synthetic procedure [50]; (ii) kinetic studies (in vitro) of the synthesized prodrugs will be performed in physiological environment, and (iii) for the prodrugs that show satisfactory properties in the in vitro studies, in vivo pharmacokinetic studies will be done in order to determine the bioavailability and the duration of action of the tested prodrugs. In light of the in vivo pharmacokinetics new prodrugs will be designed and synthesized.

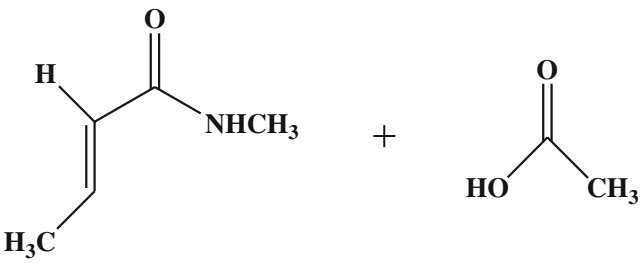

Inter

Scheme 4 Schematic representation of the intermolecular process **inter**

Acknowledgments The author would like to acknowledge funding by the German Research Foundation (DFG, ME 1024/8-1). Special thanks are also given to Nardene Karaman, Angi Karaman, Donia Karaman, and Rowan Karaman for technical assistance.

References

1. Sohi H, Sultana Y, Khar RK (2004) Taste masking technologies in oral pharmaceuticals, recent development and approaches. Drug Dev Ind Pharm 30(5):429–448
2. Reilly WJ (2002) Pharmaceutical necessities in Remington: the science and practice of pharmacy. Mack, Easton, pp 1018–1020
3. Drewnowski A, Gomez-Carneros C (2000) Bitter taste, phytonutrients, and the consumer: a review. Am J Clin Nutr 72:1424–1435
4. Hofmann T (2009) Identification of the key bitter compounds in our daily diet is a prerequisite for the understanding of the hTAS2R gene polymorphisms affecting food choice. Ann N Y Acad Sci 1170:116–125
5. Rodgers S, Busch J, Peters H, Christ-Hazelhof E (2005) Building a tree of knowledge: analysis of bitter molecules. Chem Senses 30:547–557
6. Rodgers S, Glen RC, Bender A (2006) Characterizing bitterness: identification of key structural features and development of a classification model. J Chem Inf Model 46:569–576
7. Maehashi K, Huang L (2009) Bitter peptides and bitter taste receptors. Cell Mol Life Sci 66:1661–1671
8. Behrens M, Meyerhof W (2006) Bitter taste receptors and human bitter taste perception. Cell Mol Life Sci 63:1501–1509
9. Meyerhof W, Born S, Brockhoff A, Behrens M (2011) Molecular biology of mammalian bitter taste receptors. A review. Flavour Frag J 26:260–268
10. Behrens M, Meyerhof W (2009) Mammalian bitter taste perception. Results Probl Cell Differ 47:203–220
11. Brockhoff A, Behrens M, Massarotti A, Appendino G, Meyerhof W (2007) Broad tuning of the human bitter taste receptor hTAS2R46 to various sesquiterpene lactones, clerodane and labdane diterpenoids, strychnine, and denatonium. J Agric Food Chem 55:6236–6243
12. Meyerhof W, Batram C, Kuhn C, Brockhoff A, Chudoba E, Bufe B, Appendino G, Behrens M (2010) The molecular receptive ranges of human TAS2R bitter taste receptors. Chem Senses 35:157–170
13. Wiener A, Shudler M, Levit A, Niv MY (2011) BitterDB: a database of bitter compounds. Nucleic Acids Res :1–7
14. Bufe B, Hofmann T, Krautwurst D, Raguse JD, Meyerhof W (2002) The human TAS2R16 receptor mediates bitter taste in response to beta-glucopyranosides. Nat Genet 32:397–401
15. Sainz E, Cavenagh MM, Gutierrez J, Battey JF, Northup JK, Sullivan SL (2007) Functional characterization of human bitter taste receptors. Biochem J 403:537–543
16. Sakurai T, Misaka T, Ishiguro M, Masuda K, Sugawara T, Ito K, Kobayashi T, Matsuo S, Ishimaru Y, Asakura T et al (2010) Characterization of the beta-D-glucopyranoside binding site of the human bitter taste receptor hTAS2R16. J Biol Chem 285:28373–28378
17. Ayenew Z, Puri V, Kumar L, Bansal AK (2009) Trends in harmaceutical taste masking technologies: a patent review. Recent Pat Drug Deliv Formul 3:26–39
18. Gowthamarajan K, Kulkarni GT, Kumar MN (2004) Pop the pills without bitterness taste-masking technologies for bitter drugs. Resonance 25
19. Bakan JA (1986) Microencapsulation, theory and practice of industrial pharmacy, Third edn. 412–429
20. Fawzy AA (1998) Pleasant tasting aqueous liquid composition of a bitter-tasting drug. PCT Int Appl WO9805312, 2.
21. Gowan WG (1993) Aliphatic esters as solventless coating pharmaceuticals. Can Pat Appl CA2082137:11
22. Iyer VS, Srinivas SC (2007) WO2007060682
23. Bush L (2004) Bitter taste bypass need for sugar spoon. Pharm Technol 2004.http://pharmtech.findpharma.com/pharmtech/data/articlestandard//pharmtech/072004/84521/article.pdf
24. Redondo AMJ, Abanades LB (2003) WO047550
25. Kashid N, Chouhan P, Mukherji G (2007) WO2007108010
26. www.pharmainfo.net. (2007) Ion exchange resin complex: an approach to mask the taste of bitter drugs
27. Bress WS, Kulkarni N, Ambike S, Ramsay MP (2006) EP1674078
28. Mendes WR (1976) Theory and practice of Industrial pharmacy, 3rd edn. p 346
29. Parr RG, Yang W (1989) Density functional theory of atoms and molecules. Oxford University Press, Oxford
30. Ley JP (2008) Masking bitter taste by molecules. Chem Percept 1:58–77
31. Chandreshekar J, Mueller K, Hoon MA, Adler E, Feng L, Guo W, Zuker CS, Ryba NJP (2000) T2Rs function as bitter taste receptor. Cell (Cambridge, Mass) 100:703–711
32. Scotti L, Scotti MT, Ishiki HM, Ferreira MGP, Emerenciano VP, Menezes CMS, Ferreira EI (2007) Quantitative elucidation of the structure-bittereness relationship of cynaropicrin and grosheimin derivatives. Food Chem 105:77–83
33. Menger FM, Ladika M (1988) Fast hydrolysis of an aliphatic amide at neutral pH and ambient temperature. A peptidase model. J Am Chem Soc 110:6794–6796
34. Karaman R (2010) The efficiency of proton transfer in Kirby's enzyme model, a computational approach. Tetrahedron Lett 51:2130–2135
35. Karaman R, Hallak H (2010) Anti-malarial pro-drugs- a computational aided design. Chem Biol Drug Des 76:350–360
36. Karaman R (2010) Prodrugs of aza nucleosides based on proton transfer reactions. J Comput Mol Des 24:961–970
37. Karaman R (2011) Analyzing the efficiency of proton transfer to carbon in Kirby's enzyme model—a computational approach. Tetrahedron Lett 52:699–704
38. Hejaz H, Karaman R, Khamis M (2012) Computer-assisted design for paracetamol masking bitter taste prodrugs. J Mol Model 18:103–114
39. Karaman R, Dajani KK, Hallak H (2012) Computer-assisted design for atenolol prodrugs for the use in aqueous formulations. J Mol Model 18:1523–1540
40. Karaman R (2011) Computational aided design for dopamine prodrugs based on novel chemical approach. Chem Biol Drug Des 78:853–863
41. Karaman R, Dajani KK, Qtait A, Khamis M (2012) Prodrugs of acyclovir—a computational approach. Chem Biol Drug Des 79:819–834
42. Finn A, Straugun A, Meyer M, Chubb J (1987) Effect of dose and food on the bioavailability of cefuroxime axetil. Biopharm Drug Dispos 8:519–526
43. Kees F, Lukassek U, Naber KG, Grobecker H (1991) Comparative investigations on the bioavailability of cefuroxime axetil. Arzneimittelforschung 41:84.3
44. Patel AR, Vavia PR (2008) Preparation and evaluation of taste masked famotidine formulation using drug/beta-cyclodextrin/polymer ternary complexation approach. AAPS PharmSci Tech 9(2):544–550
45. Bora D, Borude P, Bhise K (2008) Taste masking by spray-drying technique. AAPS PharmSci Tech 9(4):1159–1164
46. Yajima T, Nogata A, Demachi M, Umeki N, Itai S, Yunoki N et al (1996) Particle design for taste-masking using a spray-congealing technique. Chem Pharm Bull 44(1):187–191

47. Al-Omranm MF, Al-Suwayeh SA, El-Helw AM, Saleh SI (2002) Taste masking of diclofenac sodium using microencapsulation. J Microencapsul 19(1):45–52
48. Shidhaye S, Malke S, Kadam V (2008) Taste masked, orally disintegrating tablet containing microspheres for immediate release. J Pharm Res 1:225–229
49. Perry CM, Brogden RN (1996) Cefuroxime axetil. A review of its antibacterial activity, pharmacokinetic properties and therapeutic efficacy. Drugs 52(1):125–158
50. Kirby AJ, Lancaster PW (1972) Structure and efficiency in intramolecular and enzymatic catalysis. Catalysis of amide hydrolysis by the carboxy-group of substituted maleamic acids. J Chem Soc Perkin Trans 2:1206–1214
51. Karaman R (2011) Analyzing the efficiency in intramolecular amide hydrolysis of Kirby's N-alkylmaleamic acids—a computational approach. J Comput Theor Chem 974:133–142
52. Frisch MJ, Trucks GW, Schlegel HB, Scuseria GE, Robb MA, Cheeseman JR, Scalmani G, Barone V, Mennucci B, Petersson GA, Nakatsuji H, Caricato M, Li X, Hratchian HP, Izmaylov AF, Bloino J, Zheng G, Sonnenberg JL, Hada M, Ehara M, Toyota K, Fukuda R, Hasegawa J, Ishida M, Nakajima T, Honda Y, Kitao O, Nakai H, Vreven T, Montgomery JA Jr, Peralta JE, Ogliaro F, Bearpark M, Heyd JJ, Brothers E, Kudin KN, Staroverov VN, Kobayashi R, Normand J, Raghavachari K, Rendell A, Burant JC, Iyengar SS, Tomasi J, Cossi M, Rega N, Millam JM, Klene M, Knox JE, Cross JB, Bakken V, Adamo C, Jaramillo J, Gomperts R, Stratmann RE, Yazyev O, Austin AJ, Cammi R, Pomelli C, Ochterski JW, Martin RL, Morokuma K, Zakrzewski VG, Voth GA, Salvador P, Dannenberg JJ, Dapprich S, Daniels AD, Farkas Ö, Foresman JB, Ortiz JV, Cioslowski J, Fox DJ (2009) Gaussian 09, Revision A.1. Gaussian Inc, Wallingford
53. Casewit CJ, Colwell KS, Rappe AK (1992) Application of a universal force field to main group compounds. J Am Chem Soc 114:10046–10053
54. Murrell JN, Laidler KJ (1968) Symmetries of activated complexes. Trans Faraday Soc 64:371–377
55. Muller K (1980) Reaction paths on multidimensional energy hypersurfaces. Angew Chem Int Ed Engl 19:1–13
56. Cancès MT, Mennucci B, Tomasi J (1997) A new integral equation formalism for the polarizable continuum model: theoretical background and applications to isotropic and anisotropic dielectrics. J Chem Phys 107:3032–3041
57. Mennucci B, Tomasi J (1997) Coninuum solvation models: a new approach to the problem of solute's charge distribution and cavity boundaries. J Chem Phys 106:5151
58. Mennucci B, Cancès MT, Tomasi J (1997) Evaluation of solvent effects in isotropic and anisotropic dielectrics and in ionic solutions with a unified integral equation method: theoretical bases, computational implementation, and numerical applications. J Phys Chem B 101:10506–10517
59. Tomasi J, Mennucci B, Cancès MT (1997) The IEF version of the PCM solvation method: an overview of a new method addressed to study molecular solutes at the QM ab initio level. J Mol Struct (THEOCHEM) 464:211–226
60. Kirby AJ, Hollfelder F (2009) From enzyme models to model enzymes. Royal Society of Chemistry, 1st edn
61. Kluger R, Chin J (1982) Carboxylic acid participation in amide hydrolysis. Evidence that separation of a nonbonded complex can be rate determining. J Am Chem Soc 104:2891–2897
62. Katagi T (1990) AM1 study of acid-catalyzed hydrolysis of maleamic (4-amino-4-oxo-2-butenoic) acids. J Comput Chem 11(9):1094–1100
63. Burker U, Allinger NL (1982) Molecular mechanics. American Chemical Society, Washington, DC
64. Kirby AJ (2005) Effective molarities for intramolecular reactions. J Phys Org Chem 18:101–278
65. Karaman R, Pascal RA (2010) Computational analysis of intramolecularity in proton transfer reactions. Org Biomol Chem 8:5174–5178
66. Karaman R (2010) A general equation correlating intramolecular rates with 'attack' parameters: distance and angle. Tetrahedron Lett 51:5185–5190
67. Karaman R (2009) The *gem*-disubstituent effect—a computational study that exposes the relevance of existing theoretical models. Tetrahedron Lett 50:6083–6087
68. Karaman R (2009) The effective molarity (EM) puzzle in proton transfer reactions. Bioorg Chem 37:106–110
69. Karaman R (2010) Effects of substitution on the effective molarity (EM) for five membered ring-closure reactions—a computational approach. J Mol Struct (THEOCHEM) 939:69–74
70. Karaman R (2010) The effective molarity (EM) puzzle in intramolecular ring-closing reactions. J Mol Struct (THEOCHEM) 940:70–75
71. Karaman R (2011) The role of proximity orientation in intramolecular proton transfer reactions. J Comput Theor Chem 966:311–321